physica status solidi

pss

www.pss-journals.com

reprint

WILEY-VCH

Phys. Status Solidi B **252,** No. 9, 2129–2141 (2015) / **DOI** 10.1002/pssb.201552141

physica status solidi b
www.pss-b.com
basic solid state physics

Simplified method for the evaluation of the reverse dark current–voltage characteristic of thin film devices

Francisco A. Rubinelli* **and Marcelo De Greef**

INTEC, Universidad Nacional del Litoral, Güemes 3450, 3000 Santa Fe, Argentina

Received 17 March 2015, revised 27 May 2015, accepted 8 June 2015
Published online 24 July 2015

Keywords defect pool model, hydrogenated amorphous silicon, optical detectors, Simmons-Taylor approximation, solar cells

* Corresponding author: e-mail frubinelli@santafe-conicet.gov.ar, Phone: +54 342 455 9175, Fax: +54 342 450 944

An algorithm that simplifies the evaluation of the reverse dark current–voltage (J–V) characteristic of semiconductor thin film devices is presented. This algorithm, recognized with the symbols "0KRDA", is an approximation of the SRH formalism that can be used when the dangling bond density is modeled with either the Uniform Density Model or with the Defect Pool Model. The 0KRDA is designed to replace the 0K-Simmons–Taylor approximation (0KSTA) in reversed biased junctions operating under dark conditions. The dependence of the current density J with respect to the applied voltage V predicted with SRH formalism is well replicated by the 0KRDA. The small differences obtained in the calculated reverse dark currents can be removed by neglecting the contribution of gap states with energies closer than $kT/5$ to the intrinsic trap level. The transport physic controlling the shape of reverse dark J–V curves of thin film devices can be more easily visualized with the 0KRDA.

1 Introduction Research on non-crystalline materials has grown in the last years to become one of the most active areas in solid state physics. Silicon can be modified from the single crystalline state via a two-phase micro- or nano-crystalline state to an almost perfectly disordered amorphous state. The electronic properties that are suitable for electronic devices can be preserved by incorporating hydrogen into the network with an appropriate concentration and bonding structure.

Hydrogenated amorphous (a-Si:H) and microcrystalline (μc-Si:H) silicon thin films are currently applied to solar cells and numerous other electronic devices like radiation detectors, thin film transistors, image sensor, printing arrays, etc. The performance of these devices is highly dependent on the density of states (DOS). The a-Si:H and μc-Si:H DOS contains two different types of localized states: tail and defect states. The distributions of tail states are decreasing exponentials, one with acceptor-like states connected to the conduction band, and another with donor-like states, connected to the valence band. Defect states, originated by dangling bonds (DB), show an amphoteric character; i.e., they can have three charge states: positively, neutral, and negatively charged when unoccupied, occupied, and doubly occupied, respectively. Defect states are normally represented by three Gaussian distributions of amphoteric states recognized as D^-, D^0, and D^+ when the density is assumed uniform in each device layer (Uniform Density Model or UDM) or by the Defect Pool Model (DPM) but only in a-Si:H layers and its alloys. The DPM is based in an elaborated thermodynamic method where the creation of defects is described through specific microscopic reactions [1, 2]. No experimental evidences about its validity in the two-phase material μc-Si:H were found.

In disordered semiconductors the trapped charge density and recombination rate are usually computed by integrating the contributions of all the gap states between the valence and conduction band edges using the theory of Schockley–Read–Hall (SRH) [3, 4]. The SRH formalism describes charge trapping and recombination processes assuming that traps behave as single electron donor-like and acceptor like states; i.e, they can have only two charge states: positively charged or neutral in donor states and neutral or negatively charged in acceptor states. Simmons and Taylor derived an elegant approximation of the SRH formalism, recognized as the Simmons–Taylor Approximation (STA) [5]. The STA, valid for a continuous distribution of states, reduces the complete SRH equations to simpler expressions. This simplicity makes the physical interpretation of results easier.

In the so called "0K" Simmons–Taylor Approximation (0KSTA) the occupation functions and the recombination rate are represented by step functions. The 0KSTA was widely used in solar cell modeling because the analysis of the characteristic curves could be notably simplified [6–9].

In the DPM defect states associated with Si–Si bonds are modeled as amphoteric [1, 2] while in the UDM they are assumed either amphoteric or single states depending of the author. In this paper, they will be described as single states. A defect state is described by two correlated energy levels: one level $E^{+/0}$ related to the +/0 transition and another level $E^{0/-}$ related to the 0/− transition. The energy difference between these two levels is the correlation energy U. In either a-Si:H or μc-Si:H, amphoteric states can be described with the Decoupled State Approximation (DSA) as pairs of uncorrelated single-electron states: a donor-like level positioned at $E^{+/0}-kT\ln(2)$ and an acceptor-like level positioned at $E^{0/-}+kT\ln(2)$ [10, 11]. In these materials, the correlation energy U is much larger than the thermal energy and capture cross sections of charged states are higher than capture cross sections of neutral states. Hence, the two needed conditions to apply the DSA are fulfilled [3]. The non-equilibrium occupation functions f^+, f^0, and f^- of amphoteric states [13–15] are replaced by the SRH occupation functions f and $1-f$ for electrons and holes, respectively [16]. Trapped charge concentrations and the recombination rate obtained with the DPM can also be written in terms of decoupled states and the SRH formalism can be applied to describe the kinetics of all gap localized states. Hence, the STA and 0KSTA approximations can be applied to both tail and defect states.

In two previous papers, the current–voltage (*J–V*) characteristic curves of a-Si:H and μc-Si:H devices were first matched with the SRH formalism and afterwards re-evaluated modeling charge trapping and recombination with the STA and the 0KSTA [16, 17]. The *J–V* curves obtained with the three formalisms were compared under dark and illuminated conditions, for reverse and forward bias voltages, under different temperatures, in p–i–n devices with thinner and thicker intrinsic layers, and for different values of some key electrical parameters. Our results indicated that the STA is an acceptable approximation in p–i–n devices working under illuminated conditions for any applied voltage. Under dark conditions, the STA is valid for forward voltages and slightly overestimates the dark current of p–i–n devices subjected to reverse voltages but correctly replicating the $J(V)$ dependence. The 0KSTA is also a good approximation under illumination and dark conditions but only when forward voltages are applied. The 0KSTA cannot be used when the p–i–n device is reversed biased and operates under dark conditions [16, 17]. The errors introduced by the STA and the 0KSTA were discussed in previous contributions when the density of DBs was modeled with the UDM and the DPM [16, 17].

In this contribution, a new and simplified method is presented to evaluate the reverse dark *J–V* characteristics of a-Si:H and μc-Si:H based devices. This method that will be recognized as the "0KRDA" was conceived to replace the 0KSTA. The paper is organized as follows: in Section 2, the equations of the 0KRDA are derived; in Section 3, a detailed examination of the 0KRDA is undertaken, in Section 4, results obtained with our method and with the SRH formalism are compared for different scenarios modeling the density of states with the UDM and the DPM; in Section 5, refinements of the 0KRDA are explored to precisely reproduce the *J–V* curves obtained with the SRH and finally in our conclusions the main results are summarized.

2 0KRDA: A simplified method to evaluate the reverse dark *J–V* curves

In the SRH formalism, the occupation functions of electrons and holes, f_n and f_p and the recombination efficiency η_R are given by

$$f_n(E)=\frac{nv_{TH}\sigma_N+e_p}{nv_{TH}\sigma_N+pv_{TH}\sigma_P+e_n+e_p}, \tag{1a}$$

$$f_p(E)=\frac{pv_{TH}\sigma_P+e_n}{nv_{TH}\sigma_N+pv_{TH}\sigma_P+e_n+e_p}, \tag{1b}$$

$$\eta_R(E)=v_{TH}^2\sigma_N\sigma_P\frac{np-n_i^2}{nv_{TH}\sigma_N+pv_{TH}\sigma_P+e_n+e_p}, \tag{1c}$$

where E is the gap state energy, n and p are the free electron and hole concentrations, σ_N and σ_P are the capture cross sections for electrons and holes, v_{TH} is the thermal velocity, e_n and e_p are emission coefficients for electrons and holes, respectively, and n_i is the intrinsic concentration [4, 17]. The trap charge status of each state was not included for the sake of brevity. The emission and capture coefficients for electrons and holes can be recognized as

$$\begin{aligned} e_n &= v_{TH}\sigma_N N_C\exp\left(\frac{E-E_C}{kT}\right),\\ e_p &= v_{TH}\sigma_P N_V\exp\left(\frac{E_V-E}{kT}\right),\\ c_n &= nv_{TH}\sigma_N,\quad c_p=pv_{TH}\sigma_p,\\ c_S &= c_n+c_p, \end{aligned} \tag{1d}$$

where E_C and E_V are the conduction and valence band edges, respectively, and N_C and N_V are the conduction and valence effective density of states. The capture coefficients c_n and c_p are part of Eqs. (1a)–(1c) and c_S is their sum.

In the 0KSTA, the electron occupation functions $f_n(E)$ and $f_p(E)$ and the recombination efficiency are approximated by the following step functions [16, 17]:

$$f_n(E)=\begin{cases}1 & E_V<E<E_{fpt}\\ \dfrac{n\sigma_N}{n\sigma_N+p\sigma_P} & E_{fpt}<E<E_{fnt}\\ 0 & E_{fnt}<E<E_C\end{cases} \tag{2a}$$

$$f_p(E) = \begin{cases} 0 & E_V < E < E_{fpt} \\ \dfrac{p\sigma_P}{n\sigma_N + p\sigma_P} & E_{fpt} < E < E_{fnt} \\ 1 & E_{fnt} < E < E_C \end{cases} \quad (2b)$$

$$\eta_R(E) = \begin{cases} 0 & E_V < E < E_{fpt} \\ v_{TH}\dfrac{(np - n_i^2)\sigma_N\sigma_P}{n\sigma_N + p\sigma_P} & E_{fpt} < E < E_{fnt} \\ 0 & E_{fnt} < E < E_C \end{cases} \quad (2c)$$

where E_{fnt} and E_{fpt} are the quasi-Fermi levels for trapped electrons and trapped holes (QFLTC) defined as the energies where the following conditions are satisfied:

$$\begin{aligned} e_n(E_{fnt}) &= nv_{TH}\sigma_N + pv_{TH}\sigma_P \rightarrow E_{fnt}, \\ e_p(E_{fpt}) &= nv_{TH}\sigma_N + pv_{TH}\sigma_P \rightarrow E_{fpt}, \end{aligned} \quad (3a)$$

Equation (3a) can be rewritten by dividing the emission and capture coefficients with the thermal velocity and the capture cross sections as

$$\begin{aligned} e_{n-NOR}(E_{fnt}) &= \frac{e_n(E_{fnt})}{v_{TH}\sigma_N} = n + p\left(\frac{\sigma_P}{\sigma_N}\right) = c_{S-NOR-n}, \\ e_{p-NOR}(E_{fpt}) &= \frac{e_p(E_{fpt})}{v_{TH}\sigma_P} = n\left(\frac{\sigma_N}{\sigma_P}\right) + p = c_{S-NOR-p}. \end{aligned} \quad (3b)$$

The terms $e_{n(p)\text{-NOR}}$ and $c_{S\text{-NOR-n(p)}}$ will be recognized as the normalized emission and sum of capture coefficients c, respectively. The sub-indexes n and p indicate that capture coefficients were normalized by the product between the thermal velocity and the capture cross sections for electrons and holes, respectively. QFLTC are the energies where these normalized coefficients intersect to each other and they are given by [4]

$$\begin{aligned} E_{fnt} &= E_C + kT\ln\left(\frac{n\sigma_N + p\sigma_P}{N_C\sigma_N}\right), \\ E_{fpt} &= E_V - kT\ln\left(\frac{n\sigma_N + p\sigma_P}{N_V\sigma_P}\right). \end{aligned} \quad (3c)$$

The term n_i^2 of Eq. (2c) was not present in the original derivation of Simmons–Taylor [4]. It was added by Hack and Shur in order to obtain $\eta_R = 0$ under thermodynamic equilibrium conditions [9]. Their objective was also to improve the functioning of the STA at very low forward voltages. The total recombination rate R and the space charge density ρ can be evaluated as

$$R = \int_{E_v}^{E_c} N(E)\eta_R(E)\mathrm{d}E, \quad (4a)$$

$$\rho = \int_{E_v}^{E_c} N(E)Q(E)\mathrm{d}E, \quad (4b)$$

where $N(E)$ is the continuous density of gap states. As already stated, the 0KSTA was derived for decoupled states [5–9] where traps have either a donor or an acceptor character (DSA). The average charge $Q(E)$ and the recombination efficiency $\eta_R(E)$ in the DSA can be expressed as

$$\eta_{Rd}(E) = v_{TH}^2\sigma_N^+\sigma_P^0\frac{np - n_i^2}{nv_{TH}\sigma_N^+ + pv_{TH}\sigma_P^0 + e_n^0 + e_p^+}, \quad (5a)$$

$$\eta_{Ra}(E) = v_{TH}^2\sigma_N^0\sigma_P^-\frac{np - n_i^2}{nv_{TH}\sigma_N^0 + pv_{TH}\sigma_P^- + e_n^- + e_p^0}, \quad (5b)$$

$$Q_a(E) = qf_{na}, \quad (5c)$$

$$Q_d(E) = qf_{pd}, \quad (5d)$$

$$Q(E) = Q_d(E) - Q_a(E). \quad (5e)$$

Hence Eq. (4) can be rewritten as

$$R = \int_{E_v}^{E_c} [N_d(E)\eta_{Rd}(E) + N_a(E)\eta_{Ra}(E)]\mathrm{d}E, \quad (6a)$$

$$\rho = \int_{E_v}^{E_c} [N_d(E)Q_d(E) - N_a(E)Q_a(E)]\mathrm{d}E. \quad (6b)$$

Sub-indexes "d" and "a" refer to donor-like and acceptor-like states, respectively. The occupation functions f_{na} and f_{pd} are the expressions (1a) and (1b) with the corresponding capture cross sections for acceptor-like states and donor-like states, respectively. In Fig. 1, the dependence of the normalized emission and capture coefficients as function of the gap state energy [see Eqs. (1d) and (3b)] are shown at the center of the intrinsic layer of a p–i–n a-Si:H diode subjected to either forward or reverse voltages. Details of the device structure and the methodology used to calibrate our input parameters will be given in Section 3 [16, 17]. The intrinsic layer is 600 nm thick and the device is operating under dark conditions. In this contribution, only the parameters of the a-Si:H p–i–n intrinsic layer are shown in Table 1 for the sake of brevity. The full list of electrical parameters can be found elsewhere [16, 17].

Figure 1 shows that when the p–i–n device operates under dark conditions and subjected to a reversed voltage the QFLTC become inverted: i.e., $E_{fnt} < E_{fpt}$. This inversion makes no possible use of Eq. (2c). Hence, the conclusion

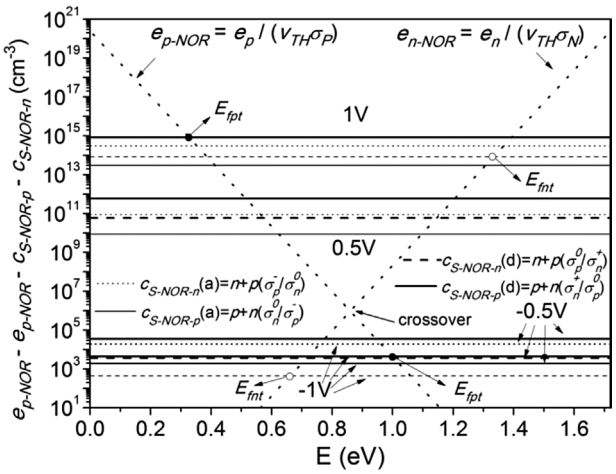

Figure 1 Normalized capture and emission coefficients of donor-like and acceptor-like defect states at half way across the intrinsic layer of an a-Si:H p–i–n device biased with voltages of ±0.5 and ±1 V. The device is operating under dark conditions and the intrinsic layer is 600 nm thick. (d) and (a) means donor and acceptor, respectively. The normalization is performed as explained in Eq. (3b). The quasi-Fermi levels for trapped carriers are indicated at 1 and −1 V for donor-like gap states only.

that the 0KSTA is not valid when the device is biased with a reverse voltage and operates under dark conditions could be inferred. However, this point requires more discussions that can be found in Section 3, where the physics of p–i–n devices operating under these conditions are further explored.

The dark current of a p–i–n diode is controlled by recombination of e–h pairs at low forward voltages and by thermal generation of e–h pairs from localized to extended states at reverse voltages. Figure 1 shows that at forward voltages emission prevail over capture at energies between the mobility edges and quasi-Fermi levels for trapped carriers, while at reverse voltages they do at energies between the quasi-Fermi levels for trapped carriers. The energy E_{T0} where the emission rates of electrons and holes $e_n(E)$ and $e_p(E)$ are equal is recognized as the intrinsic trap level. The expression of E_{T0} can be obtained from Eq. (1d) as

$$E_{T0} = \frac{E_C + E_V}{2} - \frac{kT}{2}\ln\left(\frac{\sigma_N N_C}{\sigma_P N_V}\right). \tag{7}$$

In a reverse biased, p–i–n device thermally generated electrons and holes drifted by the electric field exit the device through the back and front contact, respectively. Our simulations indicate that the dark current is originated by thermal generation of e–h pairs in the intrinsic layer and not in doped layers [18]. The e–h thermal generation rate $G(x)$ is only significant inside of some spatial region (x_1, x_2) and this region is essentially the source of the dark reverse current. The spatial co-ordinates x_1 and x_2 move toward the p/i front and i/n interfaces, respectively, at larger voltages [18]. Our simulations indicate that this region can reach doped layers

Table 1 List of electrical input parameters of intrinsic a-Si:H obtained by fitting *J–V* curves of p–i–n devices when the density of DBs is modeled with either UDM or DPM.

parameters*		parameters*	
W (nm)	600	D^+ (cm^{-3})	2×10^{15}
E_G (eV)	1.72	E_D^- (eV)	0.55
N_c, N_v (cm^{-3})	2.5×10^{20}	E_D^0 (eV)	0.85
μ_N (cm^2 V^{-1} s^{-1})	30	E_D^+ (eV)	1.15
μ_P (cm^2 V^{-1} s^{-1})	3.5	s_D (eV)	0.13
E_D (meV)	45	σ_{ngU}^+, σ_{pgU}^- (cm^2)	1.2×10^{-14}
E_A (meV)	25	σ_{ngU}^0, σ_{pgU}^0 (cm^2)	1.2×10^{-15}
σ_{nt}^+, σ_{pt}^- (cm^2)	1×10^{-15}	σ_{ngD}^+, σ_{pgD}^- (cm^2)	1×10^{-14}
σ_{nt}^0, σ_{pt}^0 (cm^2)	1×10^{-17}	σ_{ngD}^0, σ_{pgD}^0 (cm^2)	1×10^{-16}
D^- (cm^{-3})	2×10^{15}	E_{DP} (eV)	1.1
D^0 (cm^{-3})	1×10^{15}	Δ_{DP}	0.295

*The meaning of the symbols is as follows: W is the layer thickness, E_G is the mobility gap, N_c and N_v are the effective density of states in the conduction and valence band, respectively, μ_N and μ_P are the electron and hole mobilities, E_D and E_A are the valence and conduction tail slopes, σ_{nt} and σ_{pt} are the capture cross section for electrons and holes at tail states, D^-, D^0, and D^+ are the densities of states enclosed by the three Gaussians (UDM), E_D^-, E_D^0, and E_D^+ are their peak positions, and s_D is the standard deviations (UDM), σ_{ngU} and σ_{pgU} and σ_{ngD} and σ_{pgD} are the capture cross sections for electrons an holes in defect states when the UDM or the DPM, respectively, are implemented. The superscript +, 0, and − indicates the charge status. E_{DP} is the peak energy of the defect-pool, Δ_{DP} is the separation between the positive and negative charge in a-Si:H n- and p-layers. The thermal velocity v_{TH} was assumed 10^7 cm/s for both electrons and holes.

only at voltages higher than −10 V in p–i–n devices with thin intrinsic layers (200 nm or less).

In p–i–n devices, subjected to reverse voltages and operating under dark conditions the capture coefficients of Eq. (1c) can be neglected at gap state energies E between the QFLTC E_{fnt} and E_{fpt} as shown in Fig. 1. Free carrier concentrations are below their equilibrium counterparts. The electric field reinforced by the external battery pushes electrons and holes more efficiently toward contacts. Equation (1c) between the QFLTC can be expressed as

$$\eta_G(E) = -v_{TH}^2 \sigma_N \sigma_P \frac{n_i^2}{e_n + e_p}. \tag{8}$$

Emission coefficients can be written in a closer form by adopting the following convention: the trap energy E is measured positively up from E_V in the expression of the hole emission coefficient and the trap energy E^* is measured positively down from E_C in the expression of the electron emission coefficient [see Eq. (1c)]. Hence,

$$\begin{aligned} e_n &= v_{TH}\sigma_N N_C \exp\left(-\frac{E^*}{kT}\right), \\ e_P &= v_{TH}\sigma_P N_V \exp\left(-\frac{E}{kT}\right). \end{aligned} \tag{9}$$

Since the emission rates $e_n(E)$ and $e_p(E)$ exponentially decrease with the trap energy E^* or E, either $e_n(E)$ or $e_p(E)$

can be neglected few kTs away from E_{T0} as in the STA [11]. The generation rate efficiency can be re-written as:

$$\eta_G(E > E_{T0}) = -v_{TH}^2 \sigma_N \sigma_P \frac{n_i^2}{e_n},$$
$$\eta_G(E < E_{T0}) = -v_{TH}^2 \sigma_N \sigma_P \frac{n_i^2}{e_p}. \quad (10)$$

By combining Eqs. (9) and (10) the two generation efficiencies $\eta_{E<E_{T0}}$ and $\eta_{E>E_{T0}}$ can be expressed as:

$$\eta_{E<E_{T0}} = -v_{TH} n_i^2 \left(\frac{\sigma_N}{N_V}\right) \exp\left(\frac{E}{kT}\right),$$
$$\eta_{E>E_{T0}} = -v_{TH} n_i^2 \left(\frac{\sigma_P}{N_C}\right) \exp\left(\frac{E^*}{kT}\right). \quad (11)$$

The total generation rate G of e–h pairs can be obtained from Eq. (4a) as

$$G = -R \approx G_{E<E_{T0}} + G_{E>E_{T0}},$$
$$G_{E<E_{T0}} = \int_{E_{fnt}}^{E_{T0}} \eta_{E<E_{T0}}(E) N(E) dE,$$
$$G_{E>E_{T0}} = \int_{E_{fpt}^*}^{E_{T0}^*} \eta_{E>E_{T0}}(E^*) N(E^*) dE^*. \quad (12a)$$

The energies with superscripts (*) are defined as

$$E_{fpt}^* = E_G - E_{fpt},$$
$$E_{T0}^* = E_G - E_{T0}. \quad (12b)$$

The integration has been restrained to trap energies between the intrinsic trap level E_{T0} and the inverted QFLTC E_{fnt} and E_{fpt} using the same logic adopted in the 0KSTA. In Fig. 2(a) and (b), the dependence of the generation efficiency with respect to the gap state energy obtained with the SRH formalism (empty circles) and Eq. (11) (thicker solid line) are compared at the middle of the intrinsic layer of the a-Si:H p–i–n device shown in Fig. 1 (600 nm thick intrinsic layer). The other curves of Fig. 2 will be explained and discussed in Section 5. The device is biased with a reversed voltage of −1 V. The generation efficiencies were calculated with the parameters of Table 1. Figure 2(a) and (b) shows that the most significant contribution to the generation rate in the SRH formalism comes from gap states with energies between E_{fnt} and E_{fpt}, which justifies the limits of integration adopted in Eqs. (12).

As the density of states $N(E)$ is a smoother function of the gap state energy E than the emission rates $e_n(E)$ and $e_P(E)$, it can be approximated by its value at E_{T0}, i.e., $N(E) \sim N(E = E_{T0})$ and taken outside the integrals in order to simplify our expressions. The sum $e_n(E) + e_P(E)$ in Eq. (8) reaches its minimum at E_{T0}. Hence, the generation efficiency $\eta_R(E)$ reaches its maximum at E_{T0}. When the density of DBs is evaluated with the DPM, this assumption is quite accurate in the bulk of the intrinsic layer and a bit more questionable near p/i and i/n interfaces where $N(E)$ changes more rapidly with the gap energy E. However, in p–i–n junctions operating under dark conditions and subjected to reverse voltages the main contribution to the dark current comes from traps located in the bulk of the intrinsic layer and with energies near mid-gap. When the reverse voltage is increased, the region of thermal generation of e–h pairs expands toward the interfaces, but the highest contribution still comes from the intrinsic layer bulk. When the UDM is instead adopted, our approximation is valid for any applied reverse voltage. Combining Eqs. (11) and (12), the generation rates can be expressed as

$$G_{E<E_{T0}} = N(E_{T0}) \left(\frac{\sigma_N}{N_V}\right) n_i^2 kT \left[\exp\left(\frac{E_{T0}}{kT}\right) - \exp\left(\frac{E_{fnt}}{kT}\right)\right],$$

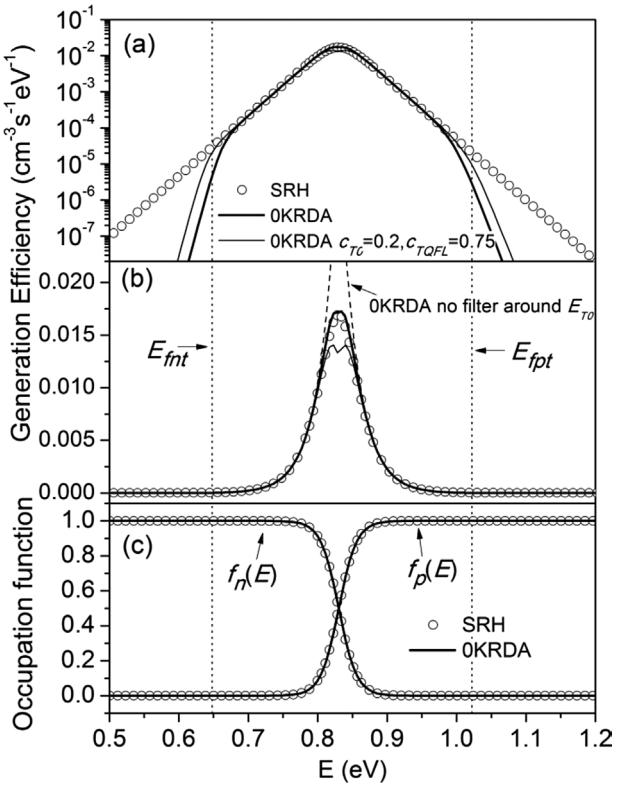

Figure 2 Generation rates as functions of the gap state energy at the middle of the 600 nm thick intrinsic layer of an a-Si:H p–i–n device reversed biased at −1 V and operating under dark conditions. Solid lines and empty circles correspond to the 0KRDA and the SRH formalisms, respectively: (a) semi-logarithmic scale and (b) linear scale. The 0KRDA is also shown when correction coefficients of $c_{T0} = 0.2$ and $c_{QFLTC} = 0.75$ at the trap intrinsic level E_{T0D}^G and quasi-Fermi levels for trapped carriers (thinner solid line) are implemented. Butterworth filters were excluded at E_{T0} in the dotted line of (b). (c) Occupation functions of electrons and holes f_n and f_p obtained with Eq. (1) (empty circles) and (16) (solid lines). All functions are shown for donor-like states.

$$G_{E>E_{T0}} = N(E^*_{T0})\left(\frac{\sigma_P}{N_C}\right)n_i^2 kT\left[\exp\left(\frac{E^*_{T0}}{kT}\right) - \exp\left(\frac{E^*_{fpt}}{kT}\right)\right]. \quad (13)$$

Replacing Eqs. (3), (7), and (12) in Eq. (13) after some algebra, the following formulas can be derived:

$$G_{E<E_{T0}} = v_{TH}\sigma_N kTn_i N(E_{T0})\left[\left(\frac{\sigma_P}{\sigma_N}\right)^{1/2} - \left(\frac{n\sigma_N + p\sigma_P}{n_i\sigma_N}\right)\right],$$

$$G_{E>E_{T0}} = v_{TH}\sigma_P kTn_i N(E_{T0})\left[\left(\frac{\sigma_P}{\sigma_N}\right)^{1/2} - \left(\frac{n\sigma_N + p\sigma_P}{n_i\sigma_N}\right)\right]. \quad (14)$$

The derivation was made for a generic density of states $N(E)$. The reverse dark current can be expressed as:

$$\begin{aligned} J(V) &= -\left(qG_{E<E_{T0}} + qG_{E>E_{T0}} + J_{e-bd} + J_{h-bd}\right) \\ &\approx -q\left(G_{E<E_{T0}} + G_{E>E_{T0}}\right). \end{aligned} \quad (15)$$

$J_{e\text{-}bd}$ is the electron back diffusion current at the front contact and $J_{h\text{-}bd}$ is hole back diffusion current at the back contact. Both terms are negligible in comparison to the first two terms $G_{E<E_{T0}}$ and $G_{E>E_{T0}}$ (q is the electron charge).

The evaluation of the trapped electron concentration requires the knowledge of the occupation function $f_n(E)$ that can be obtained by replacing the emission coefficients of Eq. (1d) in (1a) and taking into account Eq. (7). The final expression is

$$f_n(E) = \frac{1}{1 + \exp\left(2\frac{E-E_{T0}}{kT}\right)}. \quad (16a)$$

This equation is quite similar, except for the factor 2, to the occupation function of the Fermi–Dirac statistics at thermodynamic equilibrium conditions. The factor 2 makes the transition from one to zero more abrupt. The function $f_n(E)$ can be approximated by a step function that changes from one to zero at the energy level $E = E_{T0}$.

The occupation function for holes can similarly be derived as:

$$f_p(E) = \frac{1}{1 + \exp\left(2\frac{E_{T0}-E}{kT}\right)}. \quad (16b)$$

This equation can also be approximated by a step function that changes from zero to one at the energy level $E = E_{T0}$. Figure 2c shows $f_n(E)$ and $f_p(E)$ for the same electrical parameters and scenario of Fig. 2(a). When Eqs. (16) are approximated by step functions the expressions for the trapped charge densities become quite simple

$$\begin{aligned} p_T &= \int_{E_{T0}}^{E_G} N_D(E)\mathrm{d}E, \\ n_T &= \int_0^{E_{T0}} N_A(E)\mathrm{d}E. \end{aligned} \quad (17)$$

The use of Eqs. (14)–(17) that allows the evaluation of the current–voltage characteristic will be recognized as the method 0KRDA: 0K stands for the step functions used in the calculation of the generation efficiency $G(x)$ and trapped carrier concentrations $p_T(x)$ and $n_T(x)$ and RD are the initials of the author's last names. Equations (14)–(17) were implemented in our code D-AMPS, described elsewhere [19]. The different formalisms SRH, STA, 0KSTA, or 0KRDA can be selected by changing the integer value of a new input. The code D-AMPS employs the Newton–Raphson technique (NRT) to achieve convergence. The NRT iteratively finds the root of the non-linear system of three differential equations: Poisson and Continuity when an adequate initial guess is given. The NRT uses the derivates of the currents, recombination rate, and charge densities with respect to the electron potential and quasi-Fermi levels. Let's note that in the 0KRDA method, these derivatives are non zero only for the generation rate.

3 Detailed examination of the 0KRDA method The device used to test the accuracy of our approximation is the a-Si:H based p–i–n junction [16, 17]. The structure is as follows: TCO/p-a-SiC:H/i-a-Si:H/n-a-Si:H/Al with a 5 nm thick buffer layer in between the p- and i-layers. The front contact is an Asahi U-type (employing textured SnO_2:F. The p- and n-layer thicknesses are 10 and 20 nm thick, respectively. Experimental data correspond to as-deposited a-Si:H based p–i–n junctions with 200 and 600 nm thick intrinsic layers that were annealed for 30 min at 130 °C [16, 17]. These devices were grown and characterized at Delft University of Technology.

As already stated, the experimental dark and light *J–V* characteristics of a-Si:H p–i–n devices were first fitted with the SRH formalism. The absorption coefficient and the refractive index and some of the electrical parameters were obtained from thin film measurements or literature and the more difficult to measure (like capture cross sections, effective density of states, mobilities) by matching dark and illuminated *J–V* curves of a-Si:H p–i–n solar cells with different intrinsic layer thicknesses [16, 17]. For simplicity, the density of DBs was initially simulated with the Uniform Density Modeling (UDM) that assumes a constant density of DB inside of each device layer.

The density of defect states in the UDM is described with three Gaussian distributions D^-, D^0, and D^+ containing amphoteric states. They are separated in energy by 0.3 eV [1]. Amphoteric states can be approximated by donor-like and acceptor-like pairs of states as explained above. The validity of this approximation was discussed in a previous contribution [12]. In a-Si:H and μc-Si:H, three Gaussian

distributions with donor-like states and three Gaussian distributions with acceptor-like states are used to model the density of DBs. Donor-like and acceptor-like Gaussians are separated by the correlation energy U adopted equal to 0.2 eV [1, 2, 20] (see Table 1). Information about our modeling of doped layers, contacts, and device optics can be found elsewhere [16, 17].

Using the UDM in the 0KRDA, each Gaussian distribution D^+, D^0, and D^- will contribute to the generation rate with four pairs of terms [two for energies greater or lower than E_{T0} and two for donor- and acceptor-like states; see Eq. (14)] that makes a total of 12 terms. The levels E_{T0} are different for donor-like (E_{T0D}) and acceptor-like (E_{T0A}) defect states because capture cross sections σ_n and σ_p are different [Eq. (9)]. Usually E_{T0D} and E_{T0A} are the same for the three donor-like and acceptor-like Gaussians, respectively. Using the parameters of Table 1, the intrinsic trap levels at defect states can be evaluated as $E^G_{T0D} \sim 0.8$ eV and $E^G_{T0A} \sim 0.92$ eV where the supra-index was added to distinguish defect or Gaussians (G) from tail (T) states. The most significant contributions to the thermal generation rate of e–h pairs come from the acceptor-like Gaussian D^- (~39%) (peak energy = 0.75 eV) and the donor-like Gaussian D^0 (~33%) (peak energy = 0.85 eV). The second most significant contributions come from the acceptor-like Gaussian D^0 (~17%, 1.05 eV) and the donor-like Gaussian D^- (~8%, 0.55 eV). The remaining contributions originate from states of the donor-like Gaussian D^+ (~3%, 1.15 eV) and the acceptor-like Gaussian D^- (~0.02%, 1.35 eV). Percentages were evaluated at $V = -2$ V, but the proportions do not significantly change with the applied reverse voltage. These contributions are mostly determined by the proximity of the Gaussian peak energies to the energy levels E^G_{T0D} and E^G_{T0A} and in less extent by the number of states enclosed by each Gaussian. The generation efficiency changes more rapidly than the Gaussians distributions with the gap–state energy. Tail states add two more pairs of terms to the generation rate, but their contributions are negligible. Using the parameters of Table 1, the intrinsic trap levels at tail states can be evaluated as $E^T_{T0A} \sim 0.98$ eV and $E^T_{T0D} \sim 0.74$ eV. At these energies, the density of tail states is well below the density of defect (Gaussians) states, as seen in Fig. 3 where the density of defects and tail states at the energies E_{T0D} and E_{T0A} are indicated with circles.

Figure 2(a) and (b) shows that the generation efficiency of Eqs. (12) (thicker solid lines) can replicate quite well the generation efficiency obtained with the SRH formalism (empty circles) for most of the gap state energies. The decay at the QFLTC, the valley of the thinner solid line as well as the diverging dotted lines around E^G_{T0D} obtained for the generation efficiencies will be explained in Section 5. Results are illustrated for a reverse voltage of -1 V at half way of the intrinsic layer for donor-like defect states. The occupation functions f_n and f_p given by Eqs. (16) can be derived from the SRH formalism without approximations. Figure 2(c) shows, as expected, that Eqs. (16a) and (16b) give rise to identical results than Eqs. (1a) and (1b). Hence,

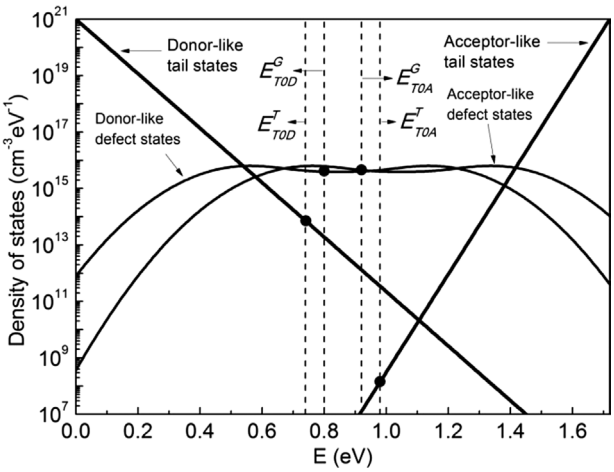

Figure 3 DOS in the intrinsic layer of the a-Si:H p–i–n device. Tail and defect states have exponential and Gaussian distributions, respectively. The total density of defect states is shown only for the sake of clarity. The intrinsic trap level E_{T0} is indicated at tail (supra-index *T*) and defect (supra-index *G*) states for donor-like (sub-index *D*) and acceptor-like states (sub-index *A*).

Fig. 2 indicate that the integration of Eqs. (11) and (16) is expected to give rise to reverse dark *J–V* similar to the ones obtained with the SRH formalism. However our results show that the implementation of the 0KRDA is not that straightforward and more discussions are needed.

In this paper, the applied reverse voltages will be considered higher or lower with respect to their absolute values. For example, applied voltages of -0.5 and -1.0 V will be considered higher and lower than -0.7 V, respectively.

Figure 4 shows that the 0KSTA follows the dark *J–V* obtained with the SRH formalism at very low reverse voltages ($V \leq -0.06$ V). On the other hand, significant differences between the predicted dark *J–V* curves obtained with the SRH and 0KSTA that steadily increase with the applied reverse voltages can be observed. The derivation of Simmons and Taylor precludes the 0KSTA of reproducing the dark *J–V* curves of p–i–n junctions when they are reversed biased [5, 16]. However, subtle details that will be now discussed open the possibility of combining the 0KSTA with the 0KRDA to properly reproducing the shape of the dark *J–V* at low reverse voltages.

When the recombination efficiencies of the 0KSTA [second line of Eq. (2c)] and the SRH formalism [Eq. (1c)] are compared, all the emission processes seem to have being neglected. However, the emission of electrons from gap states between the intrinsic trap level E_{T0} and E_{fnt} and the emission of holes from gap states between the intrinsic trap level E_{T0} and E_{fpt} are still taken into account in the 0KSTA. These emission processes are hidden in the definition of the quasi-Fermi levels for trapped carriers E_{fnt} and E_{fpt} (QFLTC).

Other inaccurate conclusion could be that the 0KSTA cannot be applied at all in reversed biased p–i–n operating

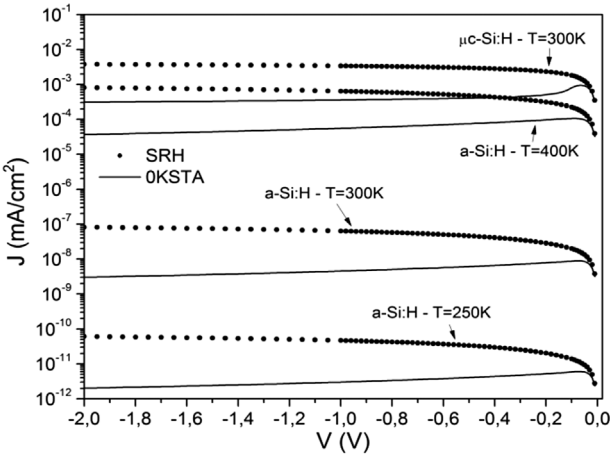

Figure 4 Comparison of the reverse dark current obtained at different temperatures with the 0KSTA and SRH formalisms for an a-Si:H p–i–n device with a 600 nm thick intrinsic layer at different temperatures. Results are also shown for a μc-Si:H p–i–n sample with a 3000 nm thick intrinsic layer at room temperature only.

under dark conditions because the QFLTC become inverted. Under dark conditions the quasi-Fermi levels of free carriers are inverted for any reverse voltage, no matter how small is. On the other hand, the QFLTC do not become inverted at very low reverse voltages. For instances, for the parameters of Table 1 the relationship $E_{fnt} > E_{fpt}$ holds over the whole intrinsic layer and Eq. (2c) can still be used for a reverse voltage of $V \sim -0.02$ V. Inversion of QFLTC in the p–i–n device under analysis begins to be observed for a reverse voltage of -0.04 V in both donor and acceptor defect states. Inverted QFLTC are found in small regions of the intrinsic region not exactly at the same spatial location and where the generation efficiency shows its maximum. At $V = -0.04$ V, the QFLTC are inverted at the left (right) hand side of the maximum of the generation rate for donor (acceptor) defects. When the reverse voltage is increased, the two regions, where QFLTC are inverted at donor-like and acceptor-like states grow and merge into only one that will be recognized with the spatial coordinates (x_3, x_4). The more the reverse voltage is increased the more similar the coordinates (x_3, x_4) are to the coordinates (x_1, x_2) where the generation rate is different from zero. Both spatial regions (x_3, x_4) and (x_1, x_2) jointly expand toward the interfaces inside the i-layer at higher reverse voltages and the relationship $x_1 \le x_3 < x_4 \le x_2$ holds.

The 0KSTA [Eqs. (2)] was implemented in D-AMPS by relying in low-pass and high-pass Butterworth filters, that will be recognized with the symbols BLP(E) and BHP(E), respectively [21]. Our code could not converge when step functions with abrupt discontinuities were directly implemented. Butterworth filters contain two parameters: the transition energy (QFLTC in our case) and the order "n" that defines its sharpness. Higher values of "n" give rise to steeper transitions. The filter order was increased until our simulations became independent of "n". In particular Eq. (2c) were realized in D-AMPS as:

$$\eta_R = \begin{cases} \eta_F \mathrm{BLP}(E_{fpt}) & E_v < E_t < E_{fpt} \\ \eta_F \mathrm{HLP}(E_{fpt})\mathrm{BLP}(E_{fnt}) & E_{fpt} < E_t < E_{fnt} \\ \eta_F \mathrm{HLP}(E_{fnt}) & E_{fnt} < E_t < E_c \end{cases}$$

$$\eta_F = v_{th} \frac{(np - n_i^2)\sigma_N \sigma_P}{n\sigma_N + p\sigma_P}. \tag{18a}$$

Butterworth filters with "n" larger than 30 behave nearly ideal filters making the recombination or generation efficiency zero at energies between the mobility edges and the QFLTC when QFLTC are not inverted [see inequalities (18b)]. On the other hand, when QFLTC become inverted the generation efficiency becomes different from zero in the energies indicated in inequalities (18c):

$$\eta_R = \begin{cases} = 0 & E_t < E_{fpt} \\ \neq 0 & E_{fpt} < E_t < E_{fnt} \\ = 0 & E_t > E_{fnt} \end{cases} \tag{18b}$$

$$\eta_R = \begin{cases} \neq 0 & E_t < E_{fpt} \\ = 0 & E_{fpt} < E_t < E_{fnt} \\ \neq 0 & E_t > E_{fnt} \end{cases} \tag{18c}$$

Under dark conditions and biasing the p–i–n junction with reverse voltages, two different scenarios are possible: (i) at very low voltages the QFLTC are not inverted along the whole intrinsic layer or (ii) at moderate and high voltages the QFLTC become inverted inside a region (x_3, x_4) of the intrinsic layer, but remaining not inverted outside of the region (x_3, x_4). In both cases, there are regions where the 0KSTA can still be applied. Our code D-AMPS checks where the QFLTC are inverted and uses the 0KRDA only inside the spatial region with coordinates (x_3, x_4). The two approximations were combined to properly describe the transport physics over the whole device length and match the dark *J–V* at any reverse voltages. When the reverse voltage is increased, the region (x_3, x_4) widens and the 0KRDA is applied to a bigger segment of the intrinsic layer. Inspection of Fig. 4 indicates that the contribution of the 0KSTA to the total current density J is ~10% (20%) of the current density obtained with the SRH formalism at reverse voltages of -0.6 V (-0.3 V). These voltages slightly change with temperature, being a bit lower at lower temperatures.

The idea of Hack and Shur of including the term n_i^2 in the numerator of Eq. (2c) [9] can be extended at low reverse voltages in regions where the QFLTC are not inverted. The 0KSTA will add an extra contribution of e–h thermally generated (instead of extra recombination of e–h pairs [9]) to the dark current because in these regions the term n_i^2 of Eq.

(2c) will prevail over the product np. On the top of that, the use of Eq. (18a) in spatial locations where the QFLTC are inverted would allow for the inclusion of emission processes of electrons and holes from gap states with energies between the mobility edges and the QFLTC to extended states. The use of Eq. (18a) can be considered as a variation of the traditional 0KSTA proposed by Simmons–Taylor in regions where QFLTC are inverted. However the contribution of these last gap states to the dark current was found to be quite low and it can be considered negligible (see Section 5).

Figure 5 shows the QFLTC for the a-Si:H p–i–n with a 600 nm thick i-layer at reverse voltages of −0.5 and −1 V. Although, near p/i and i/n interfaces the QFLTC are not inverted and more apart from each other enclosing more gap states than in the bulk (where QFLTC are inverted), the maximum contribution to the dark current comes from the intrinsic layer bulk, where the concentrations of free electrons and holes are more comparable to each other and well below the concentration of majority carrier near the interfaces (where $n \gg p$ or $p \gg n$). Thermal emission of e–h pairs is favored when two conditions are fulfilled: gap states are near the energy E_{T0} (where emission probabilities of electrons and holes are near equal; E_{T0} coincides with mid-gap when electron and hole capture cross sections are equal) and free carrier concentrations are below n_i, so that carrier emission is favored over carrier capture. This scenario is present in the i-layer bulk and not near the p/i and i/n interfaces where one type of free carrier dominates.

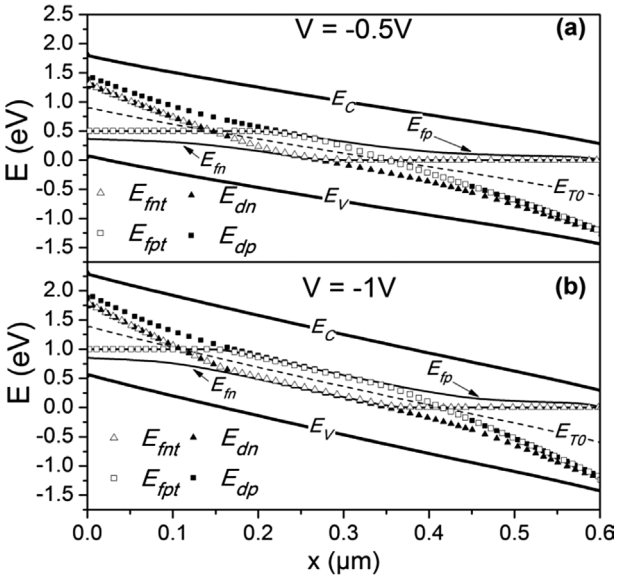

Figure 5 Band diagrams of an a-Si:H p–i–n junction with a 600 nm thick intrinsic layer obtained under dark conditions for reverse voltages of −0.5 and −1 V. The diagrams contain the conduction and valence band edges, the quasi-Fermi levels E_{fn} and E_{fp} for free carriers (solid lines), the quasi-Fermi levels for trapped carriers E_{fnt} and E_{fpt} (empty symbols), the demarcation energies E_{dn} and E_{dp} (filled symbols), and the intrinsic trap energy E_{T0}. The last five energy levels are shown for donor-like defect states.

In Fig. 6, the dark J–V curves and relative errors obtained for the 0KSTA and different variations of the 0KRDA are shown for the p–i–n device with a 600 nm thick intrinsic layer and the electrical parameters of Table 1. Hereafter the dark J–V curves obtained with the 0KRDA will include the contribution of the 0KSTA at low voltages when no clarifications are made.

4 Exploring the consistency of the 0KRDA method The accuracy of the 0KRDA method is tested by comparing the J–V curves obtained with the 0KRDA and the SRH using the same electrical and optical parameters. The closer the J–V curves are, the more accurate the method will be considered. In other words, the dark J–V obtained with the SRH formalism will be used as our reference.

Our approximation was tested modeling the density of DBs with either the UDM or the DPM in a-Si:H based p–i–n devices of different intrinsic layer thicknesses, density of defects, temperatures, and mobility gaps. Similar results and relative errors were obtained for the different scenarios. Our results are shown in Fig. 7. The relative error is only shown for the a-Si:H p–i–n with a 600 nm thick intrinsic layer at room temperature. For other devices, the relative errors are comparable. The 0KRDA was also applied to a μc-Si:H p–i–n structure with a 2000 nm thick intrinsic layer (see Fig. 7). In all cases, the approximation was found to be quite satisfactory. The 0KRDA should not be applied below 200 K because electrical transport by hopping could become significant [22]. The temperature range 200–450 K was checked in our simulations.

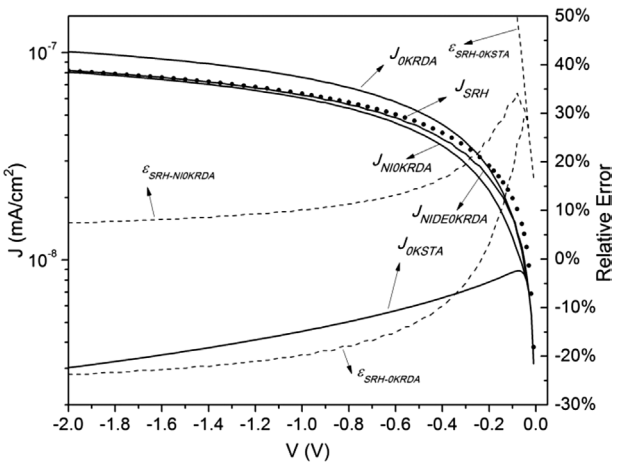

Figure 6 Comparison of the dark reverse dark J–V obtained at room temperature in the a-Si:H p–i–n sample with a 600 nm thick intrinsic layer for the formalisms: SRH (filled circles), 0KSTA and 0KRDA (solid lines). Dark J–V curves obtained with the numerical integration of the generation efficiencies are also shown for comparison: the NI0KRDA and the NIDE0KRDA where the quasi-Fermi levels for trapped carriers or the demarcation energies were adopted as integration limits, respectively (see Section 5). Errors are shown in dotted lines for some approximations.

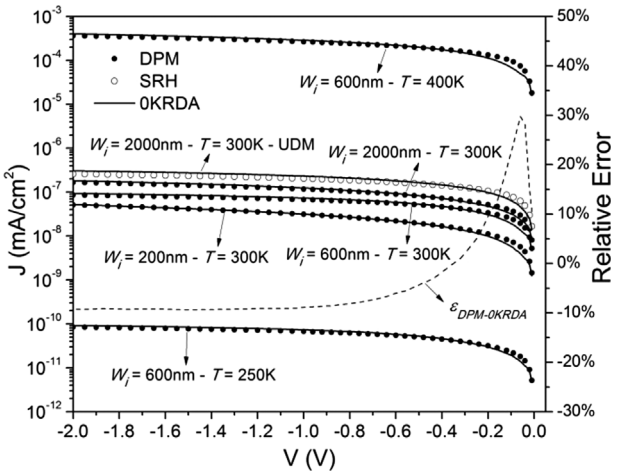

Figure 7 Comparison of the dark reverse dark *J–V* curves obtained with the SRH and 0KRDA at different temperatures and intrinsic layer thicknesses in several a-Si:H p–i–n devices where the density of DB was modeled with the DPM. The comparison is also shown for a μc-Si:H p–i–n sample with a 2000 nm thick intrinsic layer at room temperature (UDM). The relative error is shown for the a-Si:H p–i–n with a 600 nm thick intrinsic layer only.

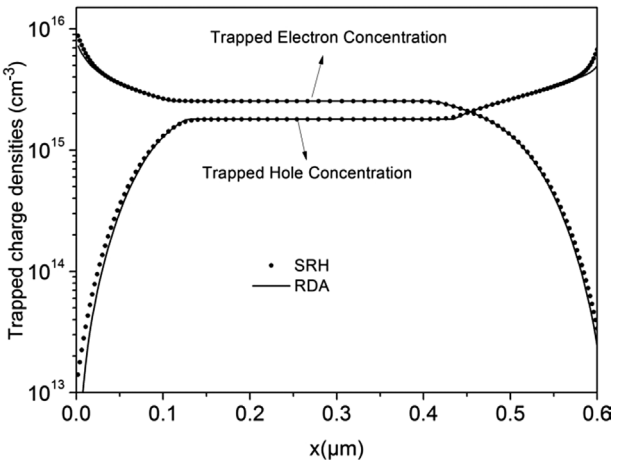

Figure 8 Trapped electron and hole concentrations obtained with the SRH and the 0KRDA formalisms for the a-Si:H p–i–n device with a 600 nm thick intrinsic layer under dark conditions at room temperature and biased with a reverse voltage of −1 V.

The 0KRDA tends to overestimate the current density J at reverse voltages higher than −0.25 V and to slightly underestimate J at low reverse voltages. However the predicted dependence of the current density J with respect to the reverse applied voltage V obtained with the SRH formalism is properly replicated. This result is similar to the one obtained for dark reversed *J–V* curves with the STA, that does not contain the step functions of the 0KSTA [17].

In the DPM, defect states are directly assumed amphoteric and represented by the energy levels $E^{+/0}$ and $E^{0/-}$ separated by correlation energy U. As the STA was derived for decoupled states the DSA was also applied to the expression of the density of DB derived by Powell and Deane [16]. Hence, the density of states $N(E)$ obtained with the DPM [1, 2] was replaced by two density of state functions: $N_d(E)$ for donor-like states, a copy of $N(E)$ located kTln(2) below in energy, and $N_a(E)$ for acceptor-like states, another copy of $N(E)$ placed above in energy by $U + \mathrm{kTln}(2)$ [2, 16].

Using the captures cross sections of Table 1 [16], obtained by matching the *J–V* characteristics with the DPM the intrinsic trap levels are again $E^G_{\mathrm{T0D}} \sim 0.74$ eV and $E^G_{\mathrm{T0A}} \sim 0.98$ eV. The freezing temperature was set to 460–K and the hydrogen concentration equal to $1 \times 10^{21}\,\mathrm{cm}^{-3}$. Other electrical parameters can be found elsewhere [16].

Similar comments about the accuracy and the combined use of both approximations (0KSTA incorporated in the 0KRDA) for the evaluation of dark reverse *J–V* curve, already made with the UDM, can be made for the DPM. However, the relative errors obtained in the evaluation of reverse dark *J–V* curves are lower when the DPM is invoked because the DSA introduces an error of opposite sign to the one originated by the STA [16].

In Fig. 8, the trapped electron and hole concentrations obtained with the SRH formalism and the 0KRDA are compared at room temperature in the a-Si:H p–i–n with a 600 nm thick i-layer when a reverse voltage of −1 V is applied modeling DBs with the UDM. Only small differences can be observed in the trapped carrier concentrations. Hence, the electric field is evaluated with a high degree of accuracy with the 0KRDA.

5 Refining the 0KRDA method Figure 6 also shows the dark *J–V* curves calculated with the option NI0KRDA that evaluates the current density with Eq. (15), but integrating the generation efficiencies of Eq. (11) numerically, instead of analytically, as follows:

$$G_{E<E_{\mathrm{T0}}} = \int_{E_{\mathrm{V}}}^{E_{\mathrm{T0}}} N(E)\eta_{E<E_{\mathrm{T0}}}(E)\mathrm{d}E \approx \sum_{i(E_{\mathrm{V}})}^{i(E_{\mathrm{T0}})} N(E_{\mathrm{i}})\eta_{E<E_{\mathrm{T0}}}(E_{\mathrm{i}})\,,$$

$$G_{E>E_{\mathrm{T0}}} = \int_{E_{\mathrm{T0}}}^{E_{\mathrm{C}}} N(E)\eta_{E>E_{\mathrm{T0}}}(E)\mathrm{d}E \approx \sum_{i(E_{\mathrm{T0}})}^{i(E_{\mathrm{C}})} N(E_{\mathrm{i}})\eta_{E>E_{\mathrm{T0}}}(E_{\mathrm{i}})\,. \tag{19}$$

Trapped charge densities are also evaluated with numerically integrations of the product between the density of states $N(E)$ and the occupation functions f_n and f_p. The dark *J–V* obtained with the NI0KRDA is closer to our reference (SRH) than its counterpart of the 0KRDA (see Fig. 6). The relative error is very low especially at reverse voltages higher than −0.8 V indicating that the 0KRDA could be improved further.

In order to realize the 0KRDA from the NI0KRDA, two steps are needed: the numerical integration must be replaced

by the analytical integration of the generation efficiency with respect to energy made in Eqs. (14) and the electron and hole occupation functions of Eqs. (16) must be approximated by step functions to evaluate trapped carrier concentrations and the electric field. In the NI0KRDA, low-pass and high-pass Butterworth filters were implemented at $E_{\rm fnt}$ and $E_{\rm fpt}$ and $E_{\rm T0}$ to realize the sharp steps and achieve convergence in D-AMPS, as it was done in the 0KSTA. Being more specific in the NI0KRDA, the following filters were defined: BHP($E_{\rm fnt}$) and BLP($E_{\rm T0}$) for energies $E_{\rm fnt} \le E \le E_{\rm T0}$ and BHP($E^*_{\rm T0}$) and BLP($E^*_{\rm fpt}$) for energies $E^*_{\rm fpt} \le E^* \le E^*_{\rm T0}$, respectively. The approximations $e_{\rm n}(E) \ll e_{\rm p}(E)$ and $e_{\rm n}(E) \gg e_{\rm p}(E)$ at energies $E < E_{\rm T0}$ and $E < E_{\rm T0}$ made in the 0KRDA and STA are quite accurate few kTs away from $E_{\rm T0}$ ($E^*_{\rm T0}$), but near $E_{\rm T0}$ ($E^*_{\rm T0}$) they become questionable as shown in Fig. 2b. The dotted line of Fig. 2b indicates how the generation efficiency of our 0KRDA increases significantly over the one of the SRH near $E_{\rm T0}$ ($E^*_{\rm T0}$) reaching a maximum value of 0.031 (dotted line) that can be visualized in the linear scale adopted in Fig. 2b (the value 0.031 is not shown for scale reasons). The integration of this excess of the generation efficiency gives rise to the higher density currents predicted by the 0KRDA with respect to the SRH formalism. In the NI0KRDA, the Butterworth filters incorporated at $E_{\rm T0}$ (and $E^*_{\rm T0}$) preclude the generation efficiency of reaching these excessive values as shown also in Fig. 2b (see solid thicker line). The numerical integration was performed by sub-dividing the mobility in equally spaced energy slabs and the generation efficiency peaks up in the nearest slabs to $E_{\rm T0}$ (and $E^*_{\rm T0}$).

In order to test how sensitive is the 0KRDA to the limits of integration of Eqs. (12), $E_{\rm T0}$ and $E^*_{\rm T0}$ were replaced by $E_{\rm T0} - c_{\rm T0}kT$ and $E^*_{\rm T0} - c_{\rm T0}kT$ where "$c_{\rm T0}$" is an adjustable constant. Figure 9(a) shows the obtained dependence of dark J–V curves with the constant "$c_{\rm T0}$". The dark J–V curves predicted with the 0KRDA and the SRH are on the top of each other at high reverse voltages and the relative errors are considerably reduced when the constant $c_{\rm T0}$ is adopted equal to $c_{\rm T0} = 0.2$; i.e, by restraining the analytical integration to one fifth of kT at both sides of the energy $E_{\rm T0}$. The valley observed in Fig. 2b (see thinner solid line) is created by the filters BLP($E_{\rm T0}$) and BHP($E^*_{\rm T0}$) when $c_{\rm T0}$ is 0.2. On the other hand, the drops at the QFLTC showed in Fig. 2a (solid lines) are caused by the filters BHP($E_{\rm fnt}$) and BLP($E^*_{\rm fpt}$). Hence, at low reverse voltages, the agreement with the J–V predicted with the SRH can also be improved by introducing another adjustable constant "$c_{\rm QFLTC}$" in order to extend the region of integration a little beyond the inverted QFLTC. Introducing this new adjustable constant, $E_{\rm fnt}$ and $E_{\rm fpt}$ are replaced by the energies $E_{\rm fnt} - c_{\rm QFLTC}kT$ and $E^*_{\rm fpt} - c_{\rm QFLTC}kT$. The best fit was achieved for $c_{\rm QFLTC} \sim 0.75$. Using this new correction the predicted dark J–V curves with 0KRDA and SRH are nearly on the top of each other at low reverse voltages also.

One more elegant approach to refine our approximation was also investigated. The QFLTC $E_{\rm fnt}$ and $E_{\rm fpt}$ of Eqs. (12) and (13) were replaced by the demarcation energies (DE) defined by Rose [23]. DEs are the energies where an electron or hole has the same probability of being emitted to the conduction or valence band, respectively, than to recombine; i.e., where the following conditions are fulfilled:

$$e_{\rm n} = pv_{\rm TH}\sigma_{\rm P},$$
$$e_{\rm p} = nv_{\rm TH}\sigma_{\rm N}.$$

The DE for electrons and holes are given by [23]

$$E_{\rm dn} = E_{\rm C} + kT\ln\left(\frac{p\sigma_{\rm P}}{N_{\rm C}\sigma_{\rm N}}\right),$$
$$E_{\rm dp} = E_{\rm V} - kT\ln\left(\frac{n\sigma_{\rm N}}{N_{\rm V}\sigma_{\rm P}}\right). \qquad (20)$$

When the QFLTC are replaced by $E_{\rm dn}$ and $E_{\rm dp}$ the generation rate expressions change to [see Eq. (14)]:

$$G_{E<E_{\rm T0}} = v_{\rm TH}\sigma_N kTn_{\rm i}N(E_{\rm T0})\left[\left(\frac{\sigma_{\rm P}}{\sigma_{\rm N}}\right)^{1/2} - \left(\frac{p\sigma_{\rm P}}{n_{\rm i}\sigma_{\rm N}}\right)\right],$$

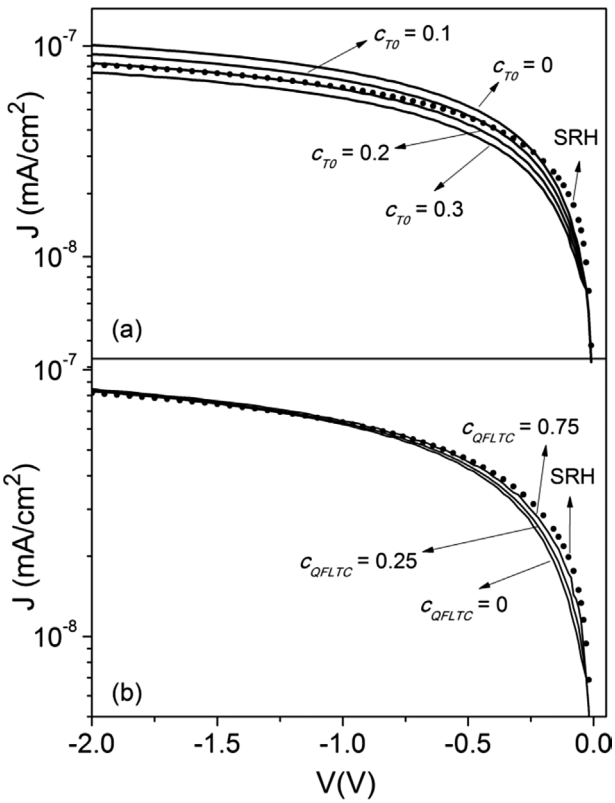

Figure 9 Changes in the predicted reverse dark J–V curves obtained in the a-Si:H p–i–n sample with a 600 nm thick intrinsic layer at room temperature when the integration limits are changed as follows: (a) $E_{\rm T0}$ is replaced by $E_{\rm T0} - c_{\rm T0}kT$ and $E^*_{\rm T0} - c_{\rm T0}kT$; (b) $E_{\rm fnt}$ and $E_{\rm fpt}$ are replaced by $E^*_{\rm fnt} - c_{\rm QFLTC}kT$ and $E^*_{\rm fpt} - c_{\rm QFLTC}kT$, where $c_{\rm T0}$ and $c_{\rm QFLTC}$ are adjustable coefficients.

$$G_{E>E_{T0}} = v_{TH}\sigma_P kTn_i N(E_{T0}) \left[\left(\frac{\sigma_N}{\sigma_P}\right)^{1/2} - \left(\frac{n\sigma_N}{n_i\sigma_P}\right) \right]. \quad (21)$$

The dark *J–V* curves obtained by implementing these generation rates in Eq. (15) will be recognized as the option DE0KRDA. It is important to realize that Eq. (21) can be used only inside the spatial region where the QFLTC are inverted because outside this region both DE are either below or above the energy E_{T0} (see Fig. 5). The electron demarcation energies, like the quasi-Fermi levels, become inverted at any reverse applied voltage *V*, no matter how small is *V*. Figure 5 shows that near the crossover of QFLTC the DE and the QFLTC of minority carriers depart from each other adding more gap states to the integration performed in Eqs. (12). The dark *J–V* curves obtained with the options 0KRDA and DE0KRDA are quite similar at high reverse voltages. On the other hand at low reverse voltages the dark *J–V* obtained with the DE0KRDA becomes closer to our reference (SRH). The numerical integration using the demarcation energies was also explored in the NIDE0KRDA. Low-pass and high-pass Butterworth filters were defined at E_{dn} and E_{dp} and E_{T0} following similar procedure as in the NI0KRDA.

In either the 0KRDA or the DE0KRDA, the current density *J* would be underestimated at low reverse voltages if the 0KSTA is not implemented in parallel. Similar comments apply when the integration with respect to the gap energy [Eq. (12)] is performed numerically rather than analytically (see in Fig. 6, results with the NI0KRDA and NIDE0KRDA). In order to clearly show how important is the contribution of the 0KSTA to the dark *J–V* curves they were first reevaluated by excluding the contribution of gap states situated between inverted E_{fnt} and E_{fpt} and mobility edges and in second instances by neglecting the contribution of the 0KSTA of states from regions where QFLTC are not inverted. Figure 10 shows that in the first case differences are very minor (*J–V* curves are practically on the top of each other) but in the second case deviations at low reverse voltages are significant.

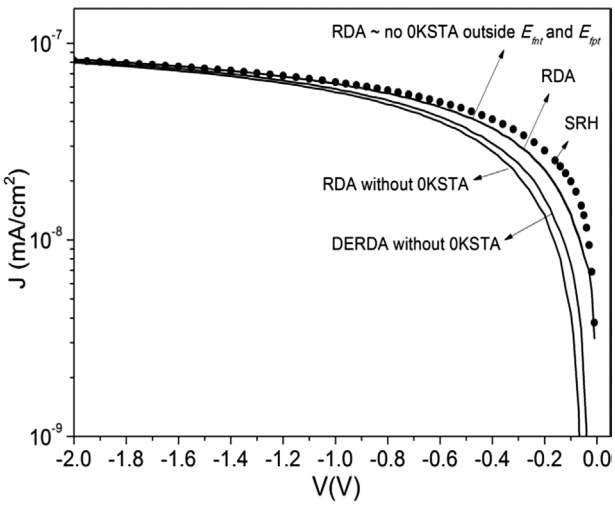

Figure 10 Comparison of dark reverse dark *J–V* curves obtained with the SRH (filled circles) and 0KRDA (solid lines) formalisms at room temperature in the a-Si:H p–i–n device with a 600 nm thick intrinsic layer. The impact of removing the contribution of the 0KSTA at states with energies between the quasi-Fermi levels for trapped carriers and the mobility edges is shown for the 0KRDA only. The full removal of 0KSTA contributions is shown for the 0KRDA and the DE0KRDA. *J–V* curves are corrected by $0.2kT$.

6 Conclusions A new algorithm, recognized as 0KRDA, that simplifies the evaluation of the reverse dark current voltage (*J–V*) characteristics of semiconductor thin film devices was developed. It was designed to replace the 0K-Simmons–Taylor approximation (0KSTA) in regions where quasi-Fermi levels for trapped carriers E_{fnt} and E_{fpt} are inverted, a scenario found in reversed biased junctions operating under dark conditions. The 0KRDA can be applied when the dangling bond density is modeled either with the Uniform Density of states Model (UDM) or the Defect Pool Model (DPM). When a p–i–n junction is subjected to low reverse voltages the 0KRDA should be combined with the 0KSTA to properly reproduce the *J–V* obtained with the SRH. Contributions to the generation of e–h pairs of gap states between the non-inverted quasi Fermi levels for trapped carriers in the intrinsic layer are not negligible. At higher reverse voltages the 0KRDA can reproduce the dependence of the current *J* with the applied voltage *V* obtained with the SRH formalism without necessity of including the contribution of the 0KSTA. The departure between the reverse dark *J–V* curves obtained with the SRH formalism and the 0KRDA for reverse voltages higher than |0.1| V is not greater than |10|% (|25|%) when the DPM (UDM) is adopted. At high reverse voltages the error can be minimized by neglecting the contribution of thermally e–h pairs from gap states located closer than $0.2kT$ of the intrinsic trap level E_{T0} while at low reverse voltages the error can be minimized by extending the region of gap states contributing to the generation of thermal e–h pairs in $0.75kT$ beyond the inverted quasi-Fermi levels for trapped carriers. The predicted dark *J–V* curve becomes closer to the one obtained with the SRH formalism at low reverse voltages also when gap states between the inverted demarcation energies rather than the quasi-Fermi levels for trapped carriers are included in the thermal generation of e–h pairs. The 0KRDA can be applied to other disordered semiconductor based detectors and solar cells devices than p–i–n junctions, like Schottky barriers, tandems structures, etc. operating under dark conditions or low light intensities. Its simpler expressions facilitate the analysis of the transport physic controlling the reverse dark current.

Acknowledgements We highly appreciate the financial support of CONICET and Agencia Nacional de Promoción Científica y Tecnológica through the grants PIP 112-201101-

01052 and PICT-2013-059. We would also like to thank members of the department Photovoltaic Materials and Devices of Delft University of Technology, the Netherlands, for providing us of valuable experimental information.

References

[1] M. Powel and S. Deane, Phys. Rev. B **48**, 10815 (1993).
[2] M. Powel and S. Deane, Phys. Rev. B **53**, 10121 (1996).
[3] R. N. Hall, Phys. Rev. **87**, 387 (1952).
[4] W. Shockley and W. T. Read, Phys. Rev. **87**(5), 835 (1952).
[5] J. G. Simmons and G. W. Taylor, Phys. Rev. B **4**(2), 502 (1971).
[6] M. Hack and M. Shur, IEEE Electron Device Lett. **4**(5), 140 (1983).
[7] M. Hack and M. Shur, J. Appl. Phys. **54**(10), 5858 (1983).
[8] M. Hack and M. Shur, IEEE Trans. Electron Devices **31**(5), 539 (1984).
[9] M. Hack and M. Shur, J. Appl. Phys. **58**(2), 997 (1985).
[10] V. Halpern, Philos. Mag. B **54**, 473 (1986).
[11] V. Suntharalingam and H. M. Branz, Mater. Res. Soc. Symp. Proc. **336**, 153 (1994).
[12] E. Klimovsky, J. K. Rath, R. E. I. Schropp, and F. A. Rubinelli, Thin Solid Films **422**, 211 (2002)
[13] C. Sah and W. Shockley, Phys. Rev. **109**(4), 1103 (1958).
[14] H. Okamoto and Y. Hamakawa, Solid State Commun. **24**, 23 (1977).
[15] F. Vaillant and D. Jousse, Phys. Rev. B **34**, 4088 (1986).
[16] M. G. De Greef and F. A. Rubinelli, Phys. Status Solidi B **252**, 170 (2015)
[17] M. De Greef, F. Rubinelli, and R. A. C. M. M. van Swaaij, Thin Solid Films **540**, 227 (2013).
[18] F. Rubinelli, J. Arch, and S. Fonash, J. Appl. Phys. **72**, 1621 (1992).
[19] F. Rubinelli, J. Rath, and J. Schropp, J. Appl. Phys. **89**, 4010 (2001).
[20] G. Schumm, Phys. Rev. B **41**, 2427 (1994).
[21] R. C. Gonzalez and R. E. Woods, Digital Image Processing, 2nd edn. (Prentice Hall, New Jersey, 2002), chap. 5.
[22] R.A. Street, Hydrogenated Amorphous Silicon (Cambridge University Press, Cambridge, 1991), p. 273.
[23] A. Rose, Concepts in Photoconductivity and Allied Problems (Robert E. Krieger Publising, New York, 1978).